

Interactions of Bacterial Quorum Sensing Signals with Model Lipid Membranes: Influence of Acyl Tail Structure on Multi-Scale Response

Curran G. Gahan,¹ Reid C. Van Lehn,^{1,*} Helen E. Blackwell,^{2,*} and David M. Lynn^{1,2,*}

¹*Department of Chemical and Biological Engineering, University of Wisconsin–Madison, 1415 Engineering Dr., Madison, WI 53706, USA;* ²*Department of Chemistry, University of Wisconsin–Madison, 1101 University Ave., Madison, WI 53706, USA; Email: (R.C.V.) vanlehn@wisc.edu; (H.E.B.) blackwell@chem.wisc.edu (D.M.L.) dlynn@engr.wisc.edu*

ABSTRACT: Many common bacteria use amphiphilic *N*-acyl-L-homoserine lactones (AHLs) as signaling molecules to coordinate group behaviors at high cell densities. Past studies demonstrate that AHLs can adsorb to and promote the remodeling of lipid membranes in ways that could underpin cell-cell or host-cell interactions. Here, we report that changes in AHL acyl tail group length and oxidation state (e.g., the presence or absence of a 3-oxo group) can lead to differences in the interactions of eight naturally occurring AHLs in solution and in contact with model lipid membranes. Our results reveal the presence of a 3-oxo group to impact remodeling when AHLs are placed in contact with supported lipid bilayers (SLBs) of the phospholipid DOPC. Whereas AHLs that have 3-oxo groups generally promote the formation of microtubules, AHLs that lack 3-oxo groups generally form hemispherical caps on the surfaces of SLBs. These results are interpreted in terms of the time-scales on which AHLs translocate across bilayers to relieve asymmetrical bilayer stress. Quartz crystal microbalance with dissipation (QCM-D) measurements also reveal 3-oxo AHLs to associate with DOPC bilayers to a greater extent than their non-3-oxo analogs. In contrast, we observed no monotonic relationship between AHL tail length and bilayer reformation. Finally, we observed 3-oxo AHLs to facilitate greater transport or leakage of molecular cargo across the membranes of DOPC vesicles relative to AHLs without 3-oxo groups, also suggesting increased bilayer disruption and destabilization. These fundamental studies hint at interactions and associated multi-scale phenomena that may inform current interpretations of the behaviors of AHLs in biological contexts. These results could also provide guidance useful for the design of new classes of synthetic materials (e.g., sensor elements or drug delivery vehicles) that interact with or respond selectively to communities of bacteria that use 3-oxo AHLs for cell-cell communication.

Introduction

Quorum sensing (QS) is a cell-cell signaling process used by many common bacteria to assess population density and coordinate group behaviors at high cell numbers, including the production of virulence factors and the formation of bacterial biofilms that are detrimental and costly in clinical, commercial, and industrial settings.¹⁻⁷ QS is controlled by the production and dissemination of chemical signals that are often assumed to diffuse freely amongst individual cells in a bacterial community.^{2, 5, 8} The structures of these signals can vary widely among species,^{2, 9} and some species can produce more than one signal,¹⁰ or even several classes of signals,⁸ to regulate group behavior. While Gram-positive bacteria generally use peptide-based signals to modulate QS,^{9, 11} certain Gram-negative bacteria, including common pathogens such as *Pseudomonas aeruginosa*, use small-molecule signals known as *N*-acyl-L-homoserine lactones (AHLs).^{2, 8, 12} AHLs, as a class of signal, are shared across many different species of bacteria, and while they all have a conserved homoserine lactone (HL) head group, the structures of their acyl tails vary significantly. The impact of AHL structure on binding to their cognate intracellular receptors (i.e., LuxR-type proteins) is, in many cases, well characterized, and is believed to underpin the specificity of both intra-species and inter-species communication in bacteria.^{8, 12-15} In this paper, we report that key changes in the tail group structures of many naturally occurring AHLs can also have substantial impacts on other important physicochemical behaviors, including self-association in aqueous solution and the nature of their interactions with model lipid membranes.

The work reported here was motivated by a growing body of work demonstrating that the amphiphilic nature of AHLs can lead to self-assembly in solution and at interfaces.¹⁶⁻²⁵ The HL ‘head’ group and the acyl ‘tail’ group of varying length and structure (e.g., ranging from 4-20

carbons, oxidation state in the 3-position, etc.) provide polar and hydrophobic motifs, respectively (Figure 1).^{2, 12} This general structure resembles those of many other non-ionic amphiphiles and, provided that the tail groups are sufficiently long, can confer surface activity and resulting behaviors that are similar to those of other natural and synthetic surfactants. For example, we²³ and others¹⁸ have reported that medium to long-chained AHLs (e.g., with aliphatic tails ranging in length from 8–16 carbons; Figure 1) can self-assemble into micelles or small vesicles in aqueous solution. Daniels et al. also demonstrated that some long-chained AHLs can self-assemble and undergo phase changes when compressed at air-water interfaces.¹⁶ Finally, recent reports have demonstrated that AHLs can intercalate into lipid membranes,^{19, 20} allowing

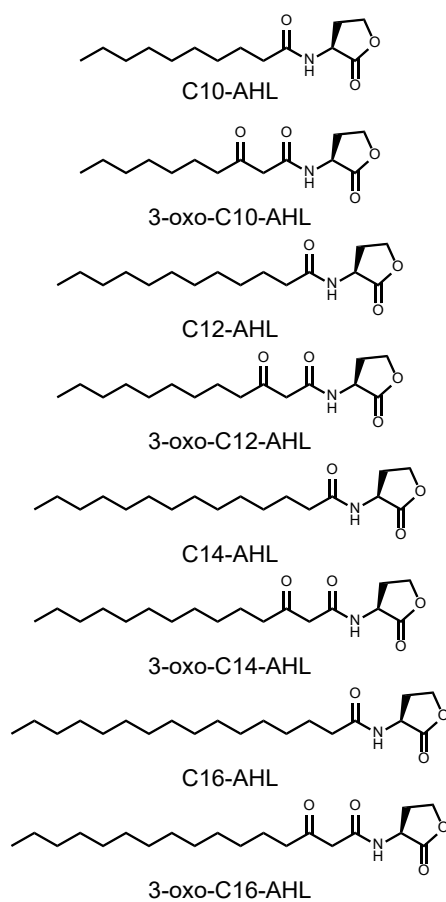


Figure 1: Chemical structures of the AHLs examined in this study.

them to translocate across lipid bilayers,²¹ promote membrane depolarization,¹⁷ dissolve lipid phases²² and, of particular interest to the work reported here, promote large-scale membrane remodeling.²⁵ These past studies reveal that both head group and aliphatic tail structure can have substantial impacts on the behaviors of AHLs, including self-association in solution^{18, 23} and adsorption to^{19, 20} and subsequent multi-scale phenomena^{17, 22, 25} that occur when they come in contact with lipid bilayers. Overall, this growing understanding of the physicochemical properties of AHLs and the richness of behaviors in which they can engage provides insight into potential additional roles, beyond simple ligand-receptor interactions, that these signaling molecules could play in facilitating bacterial communication. These past studies also suggest roles that AHLs could play in mediating interactions with eukaryotic host cells or with other self-assembled synthetic materials, such as lipid membranes commonly used as vehicles for drug delivery.

We recently reported that 3-oxo-C12-AHL (Figure 1), a naturally occurring long-tailed AHL produced by *P. aeruginosa* and other related bacteria, can promote the formation of extended microtubules and large hemispherical caps on the surfaces of model lipid bilayers formed using the phospholipid DOPC.²⁵ That study also showed that 3-oxo-C12-HS—the anionic head-group hydrolysis product of 3-oxo-C12-AHL that arises naturally in *P. aeruginosa* cultures,^{26, 27} but is biologically inactive as a modulator of QS—can also promote large scale remodeling, but in ways that differ substantially from those promoted by the non-ionic parent molecule 3-oxo-C12-AHL.²⁵ The work reported here sought to systematically investigate and characterize the impacts of AHL tail group structure on self-assembly and interactions with model lipid membranes using a family of natural AHLs produced by several different species of Gram-negative bacteria (Figure 1).¹²

In the sections below, we report qualitative and quantitative characterization of model supported lipid bilayers (SLBs) of DOPC in contact with eight different, but structurally related AHLs with tail lengths of 10–16 carbons. Characterization by fluorescence microscopy and quartz crystal microbalance with dissipation (QCM-D) reveal each of these long-tailed AHLs to promote some form of significant large-scale membrane remodeling, with the type and extent of remodeling observed to vary substantially with changes in both tail length and chemical structure (e.g., with the presence or absence of a 3-oxo substituent in the tail). The results of additional dye-leakage assays using large unilamellar vesicles (LUVs) composed of DOPC also reveal AHL structure to play a role in facilitating the transport of molecular cargo across unsupported lipid membranes similar to those used in drug delivery and many sensing applications. The results of this study thus bear on fundamental questions related to processes that bacteria may use to communicate or control host-cell response, and provide guidance that could prove useful for the design of synthetic materials and self-assembling systems that respond to or communicate with bacterial communities.

Materials and Methods

Materials. Sodium chloride (NaCl), calcein, sodium hydroxide (NaOH), dimethylsulfoxide (DMSO), triethylphosphine oxide, chloroform, Sephadex G-50, and deuterium oxide (D₂O) and 3-oxo-C14-AHL were purchased from Sigma (St. Louis, MO). C16-AHL was purchased from Santa Cruz Biotechnology (Dallas, TX). Isopropanol (iPrOH) was purchased from Fisher Scientific (Waltham, MA). 1,2-Dioleoyl-sn-glycero-3-phosphocholine (DOPC), 1,2-dihexanoyl-sn-glycero-3-phosphocholine (DHPC), filter supports, and a Mini-prep extruder were obtained from Avanti Polar Lipids (Alabaster, AL). Lissamine rhodamine B 1,2-dipalmitoyl-sn-glycero-3-

phosphoethanolamine, triethylammonium salt (Rho-DPPE) was purchased from Invitrogen (Carlsbad, CA). Sodium dodecyl sulfate (SDS) was obtained from Fisher Scientific (Pittsburgh, PA). Triton-X100 was purchased from Promega (Madison, WI). (*N*-Morpholino)propanesulfonic acid (MOPS) was obtained from MP Biomedical (Irvine, CA). Disposable culture tubes (16 × 100 mm) were acquired from VWR (West Chester, PA). Plastic centrifuge tubes (1.7 mL) were purchased from Axygen products (Tewksbury, MA). Minisort X plus 0.2 μm syringe filters were obtained from Sartorius Stedim Biotech (Goettingen, Germany). Polycarbonate extruder filters (100 nm) were obtained from Millipore (Billerica, MA). A Milli-Q system (Millipore, Bedford, MA) was used to perform deionization of distilled water yielding water with a resistivity of 18.2 MΩ. All other AHLs in this study were synthesized according to previously reported methods.^{13,}

²⁸ All materials were used as received without further purification unless otherwise specified.

Preparation of AHL Solutions. AHL stock solutions were prepared in DMSO at a concentration of 40 mM (3-oxo-C10-AHL), 20 mM (C10-AHL, 3-oxo-C12-AHL, C12-AHL, 3-oxo-C14-AHL) or 5 mM (C14-AHL, 3-oxo-C16-AHL, C16-AHL) and stored at -4 °C between uses. Immediately before experiments, aliquots of the stock solution were thawed and subsequently diluted in DMSO to 100 times the final aqueous concentration, and then further diluted 1:100 into buffer. All experiments that are described as being performed in a buffer solution were performed in 150 mM NaCl, 10 mM MOPS, pH 7.4 solution unless otherwise noted. All AHL solutions were used within one hour of initial dilution of the DMSO stocks into buffer. All aqueous solutions used in this study contained 1 vol% DMSO.

Static Light Scattering Measurements. The critical aggregation concentrations (CACs) of the AHLs used in this study were determined by static light scattering using a method described in our previous study.²³ The buffer used was filtered through a 0.22 μm filter and then centrifuged at 2000 rpm for 3 min to remove particulates and air bubbles from the buffer. AHL solutions (1.5 mL) were prepared in a 13 x 100 mm glass culture tube and allowed to sit thereafter at room temperature for 10 min. Aliquots (1.2 mL) of these samples were then transferred to a plastic cuvette and three independent measurements of the scattered light intensity were made per sample. Each measurement averaged the scattered light intensity of the sample over 5 sec time periods multiple times. Linear regression of increasing scattered light intensity with increasing AHL concentrations was used to determine the CAC of the AHL being tested. For some AHLs with longer tails, linear regressions of acquired data could not be performed with certainty. In these cases, we report estimated upper bounds of CAC values corresponding to the lowest concentration that was co-linear with values obtained at higher concentrations. Those reported values also corresponded to the lowest concentrations tested that exhibited clear deviations from background levels of scattered light intensity. For these longer-tailed AHLs, the values reported below thus represent an estimated upper bound of the CACs, and the actual CACs are likely lower than those values.

Optical Microscopy Experiments Using SLBs Formed by the Bicelle Fusion Method.

Fluorescence microscopy experiments were performed using fluorescently labeled (0.1 wt% Rho-DPPE) SLBs formed using the bicelle fusion method in Ibidi microfluidic chambers (μ -Slide VI 0.5 Glass Bottom).²⁹ The microfluidic chambers were incubated with a 1 M NaOH solution for ~30 min prior to SLB formation, followed by washing with Milli-Q H₂O and buffer

to neutralize the flow cell. DOPC and DHPC stocks in chloroform were mixed to a desired composition ($[\text{DOPC}]/[\text{DHPC}] = 0.25$), dried under a stream of N_2 , and further dried under vacuum for at least one hour. The resulting lipid film was then hydrated using buffer to produce a 1 mM bicelle suspension as determined by DOPC concentration. This suspension was iteratively immersed into an iPrOH/dry ice bath and then a warm water bath ($\sim 50^\circ\text{C}$) followed by vigorous vortexing (5 times). The resulting bicelle stock solution was diluted 1:32 to yield a solution with a DOPC concentration of 0.031 mM and then introduced to the NaOH-treated Ibidi flow cell at a flow rate of 100 $\mu\text{L}/\text{min}$. Supported lipid bilayer (SLB) formation was monitored by optical microscopy (see Video S1). Buffer was then introduced to the flow cell to wash away any remaining bicelles. The fluidity of SLBs formed using this method was characterized by performing a qualitative fluorescence recovery after photobleaching (FRAP) experiment. AHL-containing solutions were then introduced to flow cells at a flow rate of 100 $\mu\text{L}/\text{min}$, and micrographs were acquired using an Olympus IX70 inverted microscope (Center Valley, PA) and a Q-imaging EXi Aqua camera (Tucson, AZ) every 5 sec for ~ 8 min (at least 100 images). A Lumen Dynamics X-Cite Series 120PC-Q fiber-coupled mercury lamp (Monroe, LA) was used to excite fluorescently-labeled lipids using the RFP channel. To visualize changes in bilayer structure when the test AHLs were removed from solution, bilayers were subsequently washed with buffer solution at a flow rate of 100 $\mu\text{L}/\text{min}$.

Quartz Crystal Microbalance with Dissipation (QCM-D) Measurements. QCM-D measurements were performed with QSensor QSX 303 quartz crystal (QC) sensors with a fundamental frequency of 5 MHz that were coated with 50 nm of SiO_2 using a Q-Sense E4 QCM instrument (Bolin Scientific, Stockholm Sweden). Changes in the frequency ($\Delta\text{Frequency}$) and

dissipation (Δ Dissipation) of the QC sensors were monitored at the third, fifth, seventh, ninth, and eleventh overtones, and data analysis was performed using the data from the seventh overtone. An Ismatic IPC High Precision Multichannel Dispenser (Wertheim, Germany) peristaltic pump was used in all experiments to flow solutions over the crystals at 100 μ L/min. QCM-D sensors were treated with oxygen plasma for 10 min when received and then immediately immersed in a 2% SDS solution and allowed to sit in the solution for at least 30 min. The sensors were then rinsed in Milli-Q water and dried using dry nitrogen (N_2). Immediately before conducting an experiment, the sensors were again treated with oxygen plasma for 10 min and placed into the measurement apparatus, which was held at 25 ± 0.5 °C. The sensors were then allowed to equilibrate their resonance under a continuous 100 μ L/min flow of buffer solution.

For QCM-D measurements, SLBs were formed using the bicelle fusion method as described above.²⁹ Bicelle stock solutions (1 mM; as determined by DOPC concentration) were diluted to 0.031 mM in buffer and introduced to the sensor chamber. Adsorption of the bicelles to the surface and subsequent fusion were monitored by following the QCM-D traces over time. The formed bilayer was washed with buffer for \sim 20 min to remove any remaining bicelles. AHL solutions were then added to the flow chamber and allowed to interact with the bilayer for 45 min, after which the bilayer was washed with buffer for at least 45 min to observe the desorption of amphiphiles from the bilayer over time. Representative QCM-D traces are shown for a single sensor in Figure S3, and the data analysis included in sections below is the average and standard deviation of 3 or 4 ($n = 3-4$) independent experiments run simultaneously on different crystals. Immediately following each experiment, the QC sensors were immersed in a 2% SDS solution for at least 30 min, washed in Milli-Q water, and dried under N_2 gas before storage.

Fabrication of Calcein-Loaded Vesicles. Calcein-loaded large unilamellar vesicles (LUVs) were prepared using a previously described freeze-thaw and vesicle extrusion procedure.^{25, 30} In brief, DOPC dissolved in chloroform was aliquoted into vials, and the chloroform was subsequently removed under a stream of N₂ and further dried under vacuum for at least one hour. A 70 mM calcein solution in buffer was then added to the dried lipids and vortexed vigorously to form a turbid 5 mg/mL DOPC solution. The calcein-containing solution was prepared by massing an appropriate amount of calcein, to which buffer was added and the pH of the solution was adjusted to 7.4 with 10 M NaOH. The vesicle solutions were then iteratively frozen and thawed (five times) by alternatively immersing them into an iPrOH/dry ice bath and a warm water bath (~50 °C). The resulting vesicle suspension was then passed at least 11 times through a 100 nm PC filter using an Avanti Polar Lipids Mini-prep extruder producing vesicles with a hydrodynamic radius of ~130 nm, which is consistent with previously reported literature.³¹ The resulting vesicles were separated from external, unloaded calcein using a hand-packed Sephadex G-50 size exclusion chromatography column. ³¹P NMR was used to quantify the concentration of the resulting purified vesicle solution, as described previously and in the Supporting Information.³²

Calcein Leakage Assays. Calcein leakage assays were performed by combining and mixing 10 μL of a solution of calcein vesicles (at a concentration of 1 mM DOPC by monomer) with 90 μL of an AHL-containing solution in a well of a 96-well microtiter plate. The plate was allowed to sit for 5 min, after which the fluorescence intensity of the solution was measured at an excitation wavelength of 480 nm and an emission wavelength of 525 nm using a Tecan Infinite 200 Pro

plate reader. All assays were repeated in triplicate ($n = 3$) for each batch of vesicles and were performed with three ($n = 3$) different, independently produced batches of vesicles for a total of nine ($n = 9$) fluorescence measurements. Statistical significance against the buffer control or other AHL-containing solutions was determined using a one-way ANOVA with all nine normalized replicates for each condition used that was corrected for multiple comparisons using the Tukey method. The fluorescence intensity for each reading was normalized using a procedure adapted from our past study²⁵ and summarized in Equation 1, where: FI is the fluorescence intensity of the test solution, FI_{Buffer} is the fluorescence intensity of the calcein vesicles in buffer as the negative control, and $FI_{\text{TX-100}}$ is the fluorescence intensity of a vesicle solution containing 1% Triton X-100 (previously demonstrated to completely lyse vesicles at high concentrations)³³ as the positive control.

$$\text{Normalized Fluorescence} = \frac{FI - FI_{\text{Buffer}}}{FI_{\text{TX-100}} - FI_{\text{Buffer}}} \quad (\text{Eq. 1})$$

Results and Discussion

We recently reported that 3-oxo-C12-AHL can interact with model lipid membranes to form long microtubules and hemispherical caps on the surfaces of supported lipid bilayers (SLBs) and giant unilamellar vesicles (GUVs) composed of the phospholipid DOPC.²⁵ That study also demonstrated that changes in the AHL head group structure (e.g., the presence of an anionic, ring-opened homoserine moiety) can impact the nature of interactions and lead to large differences in membrane remodeling. To investigate the influence of AHL tail group structure on membrane reformation, we characterized interactions of DOPC SLBs with the set of AHLs shown in Figure 1. This family of AHLs contains differences in both the overall length (from 10 to 16 carbon atoms) and the oxidation state (the presence or absence of a 3-oxo group) of the

hydrophobic tail. We selected this subset of compounds because AHLs with acyl tail lengths in this range represent some of the most common and well-studied AHLs used by many species of bacteria.¹² In addition, AHLs with tail lengths in this range have been used in several past studies on the self-assembly of AHLs in solution and at interfaces.^{16-23, 25} These AHLs have also previously been predicted by molecular dynamics (MD) simulations to influence thermodynamic preferences for partitioning into or translocating across a lipid bilayer in ways that could influence subsequent membrane remodeling and dynamics.²⁴

To provide a basis for understanding and interpreting the behaviors of these AHLs with lipid membranes in studies described below, we first characterized the self-association of these amphiphilic compounds in aqueous solution. We previously reported the critical aggregation concentrations (CACs) of 3-oxo-C12-AHL, C12-AHL, and C16-AHL in water and bacterial growth media, as determined using measurements of static light scattering.²³ We began our studies by measuring the CACs of all eight AHLs shown in Figure 1 in the buffer (150 mM NaCl, 10 mM MOPS, 1% DMSO; pH 7.4) and general environmental conditions used in all subsequent studies of lipid membrane interactions described below (see Methods). The CACs for these AHLs are summarized in Table 1 (see Figure S1 for corresponding light scattering results). We observed characteristic signs of aggregation for all AHLs tested with the exception of 3-oxo-C10-AHL, which did not aggregate within the concentration range tested here (up to 200 μ M).

Table 1: Critical aggregation concentrations (CACs) of the AHLs shown in Figure 1.

Molecule	CAC (μM) ^{a,b}
3-oxo-C10-AHL	> 200
C10-AHL	62.4 ± 1.3
3-oxo-C12-AHL	59.5 ± 9.2
C12-AHL	1.4 ± 0.6
3-oxo-C14-AHL	3.1 ± 1.4
C14-AHL	$\leq 0.31^c$
3-oxo-C16-AHL	$\leq 0.63^c$
C16-AHL	$\leq 0.08^c$

^aThe corresponding light scattering data from which these results are derived are shown in Figure S1. ^bUnless otherwise noted, CACs were determined by linear regression of light scattering data as described in the Supporting Information. ^cEstimated value corresponding to the lowest concentration of this molecule tested that was co-linear with values obtained at higher concentrations; this value also corresponds to the lowest concentration tested that exhibited a clear deviation from background levels of scattered light intensity, however in these cases linear regressions of acquired data could not be performed with certainty; the value shown thus represents an estimated upper bound of the CAC and the actual CAC is likely lower than this value (see Materials and Methods and Supporting Information for further discussion).

The CACs measured for 3-oxo-C12-AHL, C12-AHL, and C16-AHL in this medium were similar to those reported previously (in water and bacterial culture medium; see past studies²³ for additional discussion of the self-assembly of these AHLs in solution), and the CACs for 3-oxo-C10-AHL, C10-AHL, 3-oxo-C14-AHL, C14-AHL, and 3-oxo-C16-AHL all exhibited, in general, trends in behavior similar to other classes of surfactants with respect to changes in tail length.³⁴ At each tail length, we observed the presence of a 3-oxo group to increase the CAC substantially, in some cases by as much as an order of magnitude; this general observation is similar to differences we reported for the CACs of C12-AHL and 3-oxo-C12-AHL reported previously in water and bacterial growth media.²³ Overall, these results support the view that these AHLs are amphiphilic in nature and provide a framework for interpreting their interactions with model lipid membranes, as aggregation has been previously reported to impact the

interaction of amphiphiles with lipid membranes.³⁵ We return to these results again in the discussion below.

AHL Tail Group Structure Impacts Membrane Remodeling in Supported Lipid Bilayers

We characterized the impacts of AHL tail group structure on multi-scale remodeling in DOPC SLBs formed using a recently reported bicelle fusion technique (Video S1).²⁹ We used this method, rather than the vesicle fusion method used in our past studies of membrane remodeling by 3-oxo-C12-AHL,²⁵ because it leads to SLBs that are more optically uniform than SLBs formed using vesicles.^{29, 36} To facilitate observation of bilayer reformation using fluorescence microscopy, the SLBs used here contained 0.1 wt% of the fluorescently-labeled lipid Rho-DPPE. In all experiments, SLBs were formed on the surfaces of NaOH-treated glass flow cells, and bilayer reformation was characterized by fluorescence microscopy with the direction of fluid flow oriented from the bottom to the top of each microscopy image. All initial studies were conducted using 50 μ M solutions of AHL because this concentration is just under the limit of solubility of C16-AHL, the longest-tailed AHL investigated here, in our hands.

The addition of 50 μ M 3-oxo-C12-AHL to DOPC SLBs resulted in the immediate formation of thin microtubules, some of which ultimately retracted and collapsed into hemispherical caps over a period of approximately 90 sec (Figure 2; Figure S2; Video S2). This behavior is consistent with that observed upon the introduction of 3-oxo-C12-AHL to SLBs formed using the vesicle fusion method,²⁵ suggesting that the bicelle method used to form our SLBs does not have a significant impact on the nature or extent of membrane remodeling.

Figure 2 also shows images of SLBs six min after exposure to 50 μ M solutions the other remaining AHLs (additional images at selected time points and time-lapse videos showing the

results of these experiments are provided in Figure S2 and as Supplemental Videos, respectively). Inspection of these images reveals large differences in membrane reformation as a function of tail group structure. Whereas AHLs containing a 3-oxo group in their aliphatic tails (i.e., 3-oxo-C10-AHL, 3-oxo-C12-AHL, 3-oxo-C14-AHL, and 3-oxo-C16-AHL) generally led to the growth of microtubules of varying lengths on the surface of the bilayer (many of which, again, collapsed over time into hemispherical caps), exposure to AHLs that lack a 3-oxo group in their tails (C10-AHL, C12-AHL, C14-AHL, and C16-AHL) generally led to the immediate and direct formation of structures that were similar to, but in many cases smaller and more irregularly shaped than, the hemispherical caps formed when 3-oxo compounds were introduced to the bilayer. We note that a very small number of the caps observed under these conditions appeared to result from the formation of short tubules (~5–40 μm in length) that collapsed into hemispherical caps shortly (between 5 sec and 4 min) after formation and did not otherwise persist over the timescales of the experiments described here (6 min). In addition, for AHLs containing a 3-oxo group, the extent of reformation varied qualitatively with tail length, with 3-oxo-C14-AHL leading to the most visually striking reformation and the highest areal density of tubules and hemispherical caps. We did not observe any clear qualitative correlations between tail length and the extent of bilayer reformation observed for AHLs that lack a 3-oxo group. Finally, and in general, hemispherical caps promoted by exposure to AHLs without 3-oxo groups were smaller, but far more numerous, than those promoted by AHLs containing 3-oxo groups.

Our past work on the characterization of interactions of 3-oxo-C12-AHL with DOPC SLBs²⁵ provided a framework for understanding the formation and/or retraction of microtubules

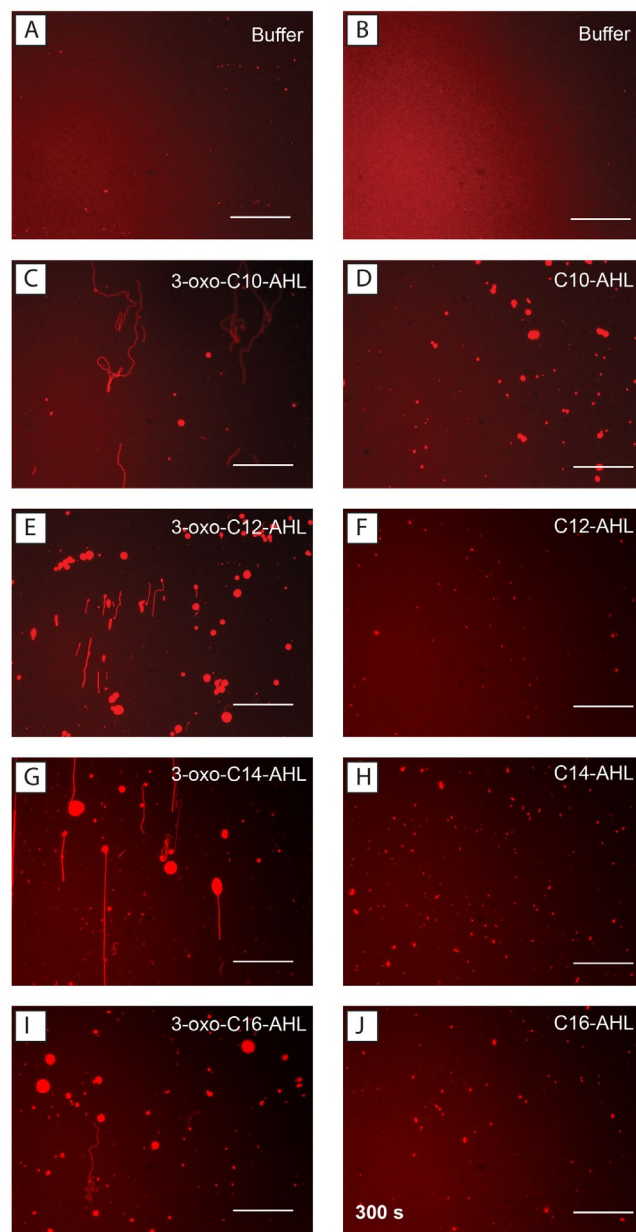


Figure 2: Representative top-down fluorescence micrographs of fluorescently-labeled DOPC SLBs that are either (A,B) stable under a continuous flow of buffer or (C-J) undergo structural reformations after exposure to a continuous flow of 50 μM solutions of (C) 3-oxo-C10-AHL, (D) C10-AHL, (E) 3-oxo-C12-AHL, (F) C12-AHL, (G) 3-oxo-C14-AHL, (H) C14-AHL, (I) 3-oxo-C16-AHL, and (J) C16-AHL. Images were acquired 360 sec after the onset of membrane restructuring, except for (J), which was acquired after 300 sec. The direction of flow in all images was from the bottom to the top of the image. Scale bars are 30 μm .

and hemispherical caps in terms of (i) the accumulation and relief of asymmetrical stresses that develop within a bilayer upon the intercalation of an amphiphile and (ii) thermodynamic barriers associated with the translocation of an amphiphile from the outer to the inner leaflet of a bilayer that alleviate these stresses. In this framework, molecules that have lower thermodynamic barriers to translocation (and that thus traverse the bilayer more rapidly) would generally be expected to promote the formation of lower-curvature hemispherical caps; molecules with higher barriers to translocation would be expected to form higher-curvature tubules as a means of relieving asymmetrical stresses between bilayer leaflets.²⁵ Molecules with intermediate barriers to translocation were proposed to form tubules that subsequently retract or collapse into hemispherical caps on the timescale during which flip-flop occurs.

Recently reported molecular dynamics (MD) simulations predict that AHLs containing 3-oxo groups in their tails generally have barriers to bilayer translocation that are approximately 5 kJ/mol higher than AHLs that lack 3-oxo groups.²⁴ These simulation predictions and the framework described above are generally consistent with the fluorescence microscopy observations reported here: AHLs containing 3-oxo groups, which have larger predicted thermodynamic barriers to translocation, generally form tubules that collapse into hemispherical caps (Figure 2; Figure S2), and the remaining AHLs, which do not contain 3-oxo groups and have lower predicted barriers to translocation, are observed to form hemispherical caps without first forming tubules. We note that differences in spontaneous curvature resulting from the presence of a 3-oxo group in the tail could also play a role in promoting the different bilayer remodeling morphologies observed here, as suggested in other studies on amphiphile-induced reformation in SLBs.³⁷ We return to consideration of AHL translocation and impacts of tail group structure on bilayer reformation again below.

Characterization of the Interactions of AHLs with DOPC Membranes Using QCM-D

The microscopy results above reveal large, qualitative differences in the remodeling of supported DOPC membranes that result from differences in both AHL tail group oxidation state and length. To provide additional quantitative insight into these differences in behavior, we used quartz crystal microbalance with dissipation (QCM-D) measurements to examine changes in structural reformation in the presence of AHLs. Figure S3 shows changes in frequency (Δ Frequency, blue line) and dissipation (Δ Dissipation, orange line) upon exposure of DOPC SLBs to AHL solutions (solid arrows) and subsequent buffer washes (dashed arrows). Each of those data sets is representative of either three or four independent replicates, the average and standard deviation of which are shown in Figure 3.

These experiments reveal that introduction of 50 μ M 3-oxo-C12-AHL to SLBs yields changes in frequency and dissipation of -2.5 ± 0.6 Hz and $1.0 \pm 0.2 \times 10^6$ (Figure 3), respectively, which is consistent with the results of our prior studies using SLBs formed by vesicle fusion.²⁵ Exposure to solutions of C12-AHL resulted in changes in frequency and dissipation of -1.3 ± 0.8 Hz and $2.5 \pm 1.0 \times 10^6$, respectively. Interestingly, we observed larger changes in frequency for 3-oxo-C12-AHL than C12-AHL, but smaller dissipation changes, a result that was unexpected because, in all previous experiments by our laboratories²⁵ and others,³⁸ if an amphiphile promotes a larger change in frequency than another, it is generally accompanied by a larger change in dissipation. This deviation from expected behavior when comparing the interactions of 3-oxo-C12-AHL and C12-AHL with SLBs could potentially arise from differences in the aggregated states of the two molecules, as C12-AHL is aggregated at 50 μ M while 3-oxo-C12-AHL is not (Table 1), a factor reported previously to alter the interactions of other

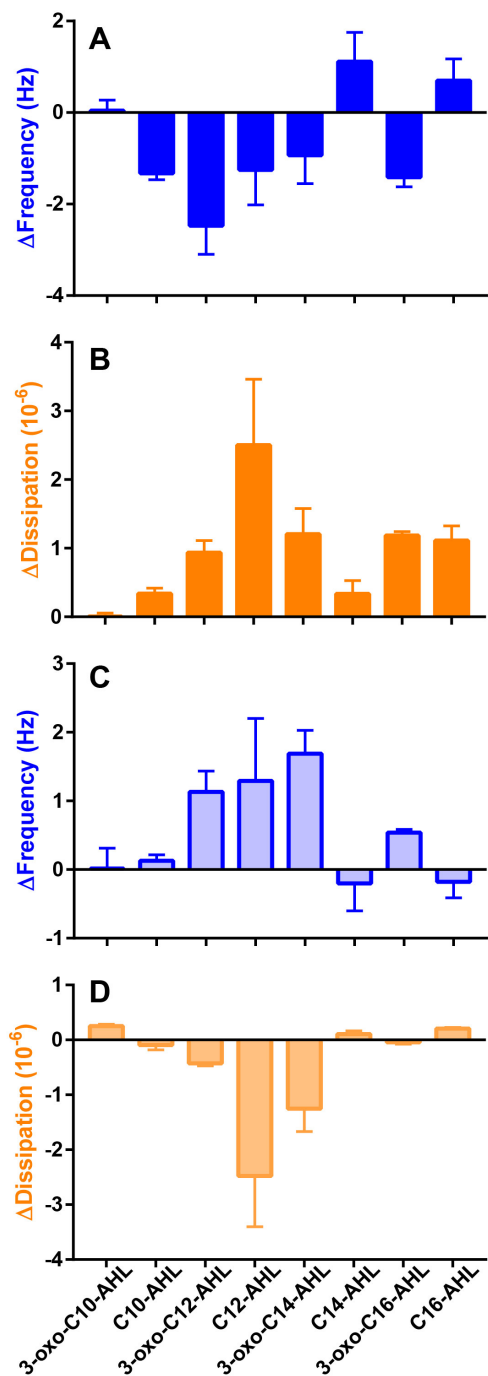


Figure 3: Changes in (A,C) frequency (Δ Frequency) and (B,D) dissipation (Δ Dissipation) for DOPC SLBs introduced to solutions of the AHLs shown in Figure 1 for 45 min (A,C) or after 45 min of buffer wash at various concentrations (B,D). The values shown are the means and a single standard deviation of three or four experiments ($n=3-4$).

amphiphiles with bilayers.^{25, 35, 39} If this is the case, the larger changes in dissipation associated with interactions of C12-AHL could result from the adsorption of aggregates of C12-AHL to the surface of the bilayer.

We next measured changes in frequency and dissipation in DOPC SLBs exposed to the remaining AHLs using QCM-D. As shown in Figure 3 and Figure S3, all of these AHLs promoted some change in both frequency and dissipation when introduced to bilayers at a concentration of 50 μM . Introduction of 3-oxo-C10-AHL and C10-AHL, which are not aggregated at this concentration (Table 1), resulted in changes in frequency and dissipation of essentially zero for 3-oxo-C10-AHL and changes of -1.3 ± 0.1 Hz and $0.3 \pm 0.1 \times 10^6$ for C10-AHL, supporting a physical picture in which C10-AHL interacts with the bilayer to a greater extent and leads to more extensive bilayer reformation. This result is again consistent with the results of MD simulations, which predict that related AHL-type compounds that do not contain 3-oxo groups can interact preferentially with lipid bilayers relative to their counterparts that do contain 3-oxo groups.²⁴

The opposite was observed when solutions of C14-AHL and 3-oxo-C14-AHL or C16-AHL and 3-oxo-C16-AHL, all of which exhibit aggregation at concentrations of 50 μM , were introduced to the bilayers. Changes in frequency and dissipation were measured to be (i) 1.1 ± 0.6 Hz and $0.3 \pm 0.2 \times 10^6$ and (ii) -0.9 ± 0.6 Hz and $1.2 \pm 0.4 \times 10^6$ for C14-AHL and 3-oxo-C14-AHL, respectively, and (iii) 0.7 ± 0.5 Hz and $1.2 \pm 0.1 \times 10^6$ and (iv) -1.4 ± 0.2 Hz and $1.2 \pm 0.1 \times 10^6$ for C16-AHL and 3-oxo-C16-AHL, respectively (Figure 3A,C and Figure S3(E-H)). These results suggest that, for AHLs with tails longer than 12 carbons, AHLs containing 3-oxo groups associate with DOPC bilayers more than their non-3-oxo counterparts. We did not observe a systematic correlation between AHL tail length and measured changes in frequency. We note

that this result contrasts with the predictions of past MD simulations discussed above; however, those simulations explicitly considered interactions with AHLs in their monomeric states, and did not account for behaviors that could arise from the presence of AHL aggregates or their potential impacts on interactions of AHLs with bilayers.²⁴ There does not appear to be any discernable monotonic relationship between AHL structure and changes in dissipation, but we did observe that AHLs with tail lengths around 12 carbons led to increased changes in dissipation relative to their longer- or shorter-chained counterparts. Subsequent washing of AHL-treated membranes with buffer (at times denoted by the locations of the dashed arrows in Figure S3 and Figure 3B,D) resulted, in most cases, in the apparent semi-reversible desorption of AHLs, indicated by changes in frequency and dissipation opposite to those observed upon initial exposure of the bilayers to AHL. We note that the differences in frequency and dissipation changes observed here could also be sensitive to changes in hydrodynamic coupling upon the interactions with AHLs with lipid bilayers; additional studies using techniques such as nano-plasmonic sensing could help further probe these interactions.⁴⁰

Taken together, these results are generally consistent with the results of our fluorescence microscopy experiments and provide support for the conclusion that the oxidation state at carbon-3 of the acyl tail can impact the interactions of AHLs with lipid bilayers significantly. Our results suggest that AHLs containing 3-oxo groups can associate with bilayers to a greater degree than their non-3-oxo counterparts, as denoted by larger frequency changes upon interaction with the bilayers. We note that our results are generally consistent with a previous report by Song et al. on the adsorption of AHLs to the membrane fraction of mammalian cells.²² In that study, the authors introduced exogenous AHLs to cultures of mammalian cells and reported the relative abundance of the AHLs in the supernatant, cytosolic, and membrane

fractions, finding increased proportions of 3-oxo-C10-AHL, 3-oxo-C12-AHL, and 3-oxo-C14-AHL to be associated with the membrane fraction, as compared to otherwise identical, non-3-oxo AHLs. Additionally, the authors observed the interaction of 3-oxo-containing AHLs with cell membranes to lead to the disruption of ordered lipid phases and, subsequently, to cell death (apoptosis). That past report suggests that changes in AHL tail group structure could play roles that extend beyond bacterial signaling, including bilayer-mediated mechanisms associated with potential inter-kingdom signaling and/or bacterial control over host-cell behaviors.²² Our results outlined here provide further support for the view that differences in AHL tail group structure—and, in particular, differences in oxidation state at the third carbon of the acyl tail—can affect large changes in the structures and dynamics of model lipid membranes.

Influence of Tail Group on Transport of Cargo Across Membranes in Lipid Vesicles

We recently reported that 3-oxo-C12-AHL can facilitate the transport of encapsulated small-molecule cargo across the unsupported lipid membranes of large unilamellar vesicles (LUVs) composed of DOPC using a well-established calcein dye leakage assay.²⁵ In that study, we observed small but significant amounts of dye leakage across membranes treated with concentrations of AHLs that also promote the formation of tubules on the surface of SLBs. That work constituted the first demonstration, to our knowledge, that this bacterial signaling molecule can promote the transport of other molecules across lipid bilayers, and suggests that dynamics associated with large-scale membrane remodeling promoted by contact with AHLs can compromise membrane barrier properties and integrity. To further interrogate this hypothesis, we conducted a final series of experiments to characterize the influence of AHL acyl tail structure, and associated changes in bilayer reformation observed above, on membrane leakage. These

experiments were performed using DOPC LUVs (vesicle diameter ~130 nm; see Materials and Methods) loaded with the self-quenching dye calcein, similar to those used in our previous study,²⁵ and measurements of fluorescence in the surrounding solution were used to characterize membrane leakage (Figure 4).

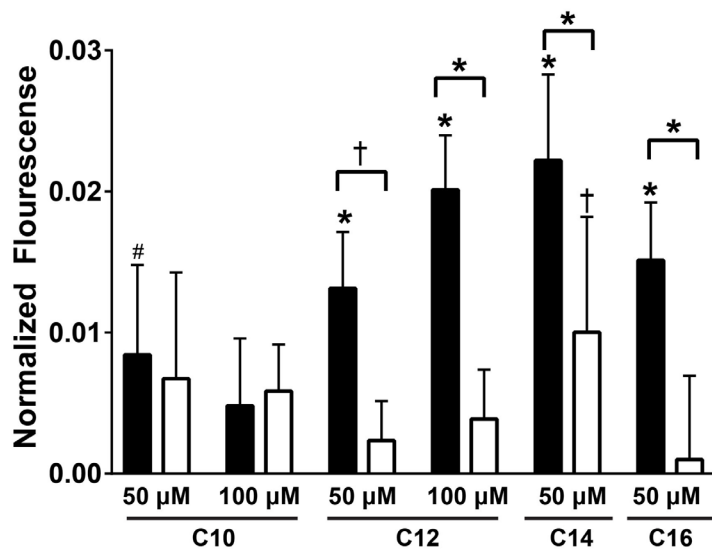


Figure 4: Normalized calcein fluorescence intensity values of solutions containing the AHLs shown in Figure 1 introduced at various concentrations to 100 μM of calcein-loaded DOPC vesicles. Black bars represent 3-oxo-containing AHLs and white bars represent non-3-oxo-containing AHLs. All values shown are the average and standard deviation of three independent experiments. (#p < 0.05, †p < 0.005, *p < 0.0005). Significance indicators above individual bars indicate significance between that condition and the buffer control; bracketed significance indicators represent significance between two AHLs that vary by the presence or absence of a 3-oxo group.

Figure 4 shows changes in normalized fluorescence over time for solutions containing calcein-loaded LUVs in contact with AHLs that either contain a 3-oxo group (filled bars) or lack a 3-oxo group (open bars). Inspection of Figure 4 reveals low but statistically significant amounts of calcein leakage when 3-oxo-C10-AHL, 3-oxo-C12-AHL, 3-oxo-C14-AHL, C14-AHL and 3-oxo-C16-AHL were introduced to LUVs. In contrast, the remaining AHLs (C10-AHL, C12-AHL, C16-AHL) promoted changes in solution fluorescence signals that were not

significantly different from those observed in our buffer controls. With the exception of 3-oxo-C10-AHL, all of the other 3-oxo AHLs promoted more leakage than their non-3-oxo counterparts. In general, these observations correlate to the nature of bilayer reformations observed and described above, with the subset of AHLs that promote the formation of tubules (which may, or may not, subsequently collapse into hemispherical caps) leading to more dye leakage.

Previous reports have demonstrated that differences in the ability of amphiphiles to translocate across a bilayer can impact the ways through which they change the permeability of or solubilize a membrane.⁴¹⁻⁴³ At lower surfactant concentrations, below the concentration at which a surfactant fully solubilizes the membrane, amphiphiles that accumulate in the outer leaflet of the membrane, and therefore lead to accumulated asymmetric bilayer strain, have been suggested to temporarily permeabilize vesicles as they translocate across the bilayer to relieve that monolayer curvature strain.^{41, 42, 44-46} Although the physical mechanism of molecular transport and leakage in our present work is not fully clear, it is likely to be related to the accumulation of monolayer curvature strain upon intercalation of AHLs that we propose, as described above, to lead to larger-scale membrane remodeling. This overall physical picture is consistent with the observation that AHLs that contain a 3-oxo group lead to dye leakage, and AHLs that lack a 3-oxo group do not. Finally, these results are interesting in the context of past reports suggesting that AHLs that contain a 3-oxo group can lead to programmed cell death²² or inhibit mammalian cell proliferation⁴⁷ at lower concentrations than their otherwise identical non-3-oxo counterparts, as highlighted above. We note that there could be several possible mechanisms through which AHLs could have an influence on cell proliferation,⁴⁸ including the membrane-facilitated apoptotic pathway described by Song et al.;²² however, our results suggest

a possibility that AHL-mediated membrane destabilization and/or reformation of host-cell membranes could also influence cell proliferation.

Conclusions

The work reported here demonstrates that differences in acyl tail group length and oxidation state can lead to large differences in the behaviors of eight structurally related bacterial AHLs in solution and in contact with model lipid membranes. Measurements of AHL aggregation in solution revealed trends with respect to tail length that are similar to those observed for other classes of amphiphiles, and that the presence of a 3-oxo group on the acyl tail substantially increased the CAC. The presence (or absence) of a 3-oxo group also has a substantial impact on the extent of large-scale membrane remodeling observed when AHLs are placed in contact with SLBs composed of the phospholipid DOPC. AHLs containing a 3-oxo group promoted the formation of tubules, some of which collapsed into hemispherical caps over time; AHLs that lack 3-oxo groups predominantly form hemispherical caps. These experimental results are in agreement with a theoretical framework proposed in past studies²⁵ suggesting that differences in the formation of tubules and caps in SLBs result from differences in the timescales on which AHLs are able to translocate across lipid bilayers to which they adsorb and, thereby, relieve asymmetrical bilayer stresses. QCM-D measurements revealed larger changes in frequency upon exposure of SLBs to solutions containing 3-oxo-AHLs relative to non-3-oxo AHLs, suggesting that AHLs containing 3-oxo groups associate with bilayers to a greater extent than their non-3-oxo counterparts. This result in the model lipid membranes used here is consistent with past observations in more complex systems that found AHLs containing 3-oxo

groups to associate with the membrane fractions of mammalian cells to a greater degree than otherwise identical AHLs lacking a 3-oxo group.²² Finally, AHLs containing 3-oxo groups facilitated greater transport of the self-quenching dye calcein across the unsupported membranes of DOPC vesicles, suggesting that the 3-oxo group may also play a role in bilayer disruption and destabilization. When combined, our results demonstrate that tail-group oxidation state can have substantial impacts on the interactions of long-chained AHLs with lipid membranes.

The results of this study on model lipid membranes hint at interactions between AHLs and lipid bilayers and several multi-scale phenomena that result from these interactions that could help provide insight into past observations on the influence of AHLs in biological contexts (e.g., to mediate bacterial cell-cell communication or inter-species host-cell interactions). In view of the dramatic changes caused by the presence of the 3-oxo group in these AHLs, it would also be interesting to examine AHLs with alternate oxidation states, such as naturally occurring 3-OH AHLs, or other non-native motifs at this position to potentially direct lipid membrane interactions toward specific desired outcomes. In this broad context, the results of this fundamental study could provide guidance for the design of new classes of synthetic materials that interact with or respond selectively to bacteria (for example, to design sensor elements or drug delivery vehicles that identify or respond differentially to communities of bacteria that use AHLs containing 3-oxo groups for communication). It is also possible that differences in bilayer reformation observed here, including the time scales over which tubules form and then collapse into caps, could, with further study, provide a basis for characterizing the relative time scales on which amphiphiles translocate across lipid bilayers. Studies to this end are currently underway and will be reported in due course.

Acknowledgements. Financial support for this work was provided by the National Science Foundation through a grant provided to the UW–Madison Materials Research Science and Engineering Center (MRSEC; DMR-1720415). The authors acknowledge the use of instrumentation supported by the NSF through the UW MRSEC (DMR-1720415). H. E. B. acknowledges support from the NIH (R35 GM131817) for this work. NMR characterization was performed in facilities in the Department of Chemistry at UW–Madison that are supported by the NSF (CHE-0342998). C. G. G. was supported in part by a NSF Graduate Research Fellowship. The authors gratefully acknowledge Samarthaben Patel and Lawrence Chen for many helpful discussions and Thomas Polaske, Dr. Kayleigh Nyffeler, Dr. Daniel Manson, and Dr. Michelle Boursier for providing many of the AHLs used in this study.

Supporting Information. Additional images, plots, and videos providing qualitative and quantitative characterization and additional associated discussion of bilayer remodeling promoted by bacterial amphiphiles (PDF). This material is available free of charge via the Internet.

ORCID

Reid C. Van Lehn: 0000-0003-4885-6599

Helen E. Blackwell: 0000-0003-4261-8194

David M. Lynn: 0000-0002-3140-8637

References

1. Daniels, R.; Vanderleyden, J.; Michiels, J., Quorum sensing and swarming migration in bacteria. *FEMS Microbiol. Rev.* **2004**, 28 (3), 261-289.

2. Waters, C. M.; Bassler, B. L., Quorum sensing: Cell-to-cell communication in bacteria. *Annu. Rev. Cell Dev. Biol.* **2005**, *21*, 319-346.
3. de Kievit, T. R., Quorum sensing in *Pseudomonas aeruginosa* biofilms. *Environ. Microbiol.* **2009**, *11* (2), 279-288.
4. Coggan, K. A.; Wolfgang, M. C., Global Regulatory Pathways and Cross-talk Control *Pseudomonas aeruginosa* Environmental Lifestyle and Virulence Phenotype. *Curr. Issues Mol. Biol.* **2012**, *14* (2), 47-69.
5. Rutherford, S. T.; Bassler, B. L., Bacterial quorum sensing: its role in virulence and possibilities for its control. *Cold Spring Harb. Perspect. Med.* **2012**, *2* (11), a012427.
6. Whiteley, M.; Diggle, S. P.; Greenberg, E. P., Progress in and promise of bacterial quorum sensing research. *Nature* **2017**, *551* (7680), 313-320.
7. Crone, S.; Vives-Florez, M.; Kvich, L.; Saunders, A. M.; Malone, M.; Nicolaisen, M. H.; Martinez-Garcia, E.; Rojas-Acosta, C.; Gomez-Puerto, M. C.; Calum, H.; Whiteley, M.; Kolter, R.; Bjarnsholt, T., The environmental occurrence of *Pseudomonas aeruginosa*. *APMIS* **2020**, *128* (3), 220-231.
8. Papenfort, K.; Bassler, B. L., Quorum sensing signal-response systems in Gram-negative bacteria. *Nat. Rev. Microbiol.* **2016**, *14* (9), 576-588.
9. Ng, W. L.; Bassler, B. L., Bacterial quorum-sensing network architectures. *Annu. Rev. Genet.* **2009**, *43*, 197-222.
10. Welch, M.; Mikkelsen, H.; Swatton, J. E.; Smith, D.; Thomas, G. L.; Glansdorp, F. G.; Spring, D. R., Cell-cell communication in gram-negative bacteria. *Mol. BioSyst.* **2005**, *1* (3), 196-202.
11. Thoendel, M.; Kavanaugh, J. S.; Flack, C. E.; Horswill, A. R., Peptide Signaling in the Staphylococci. *Chemical Reviews* **2011**, *111* (1), 117-151.
12. Fuqua, C.; Greenberg, E. P., Listening in on bacteria: Acyl-homoserine lactone signalling. *Nat. Rev. Mol. Cell Biol.* **2002**, *3* (9), 685-695.
13. Moore, J. D.; Rossi, F. M.; Welsh, M. A.; Nyffeler, K. E.; Blackwell, H. E., A Comparative Analysis of Synthetic Quorum Sensing Modulators in *Pseudomonas aeruginosa*: New Insights into Mechanism, Active Efflux Susceptibility, Phenotypic Response, and Next-Generation Ligand Design. *J. Am. Chem. Soc.* **2015**, *137* (46), 14626-14639.
14. Boursier, M. E.; Moore, J. D.; Heitman, K. M.; Shepardson-Fungairino, S. P.; Combs, J. B.; Koenig, L. C.; Shin, D.; Brown, E. C.; Nagarajan, R.; Blackwell, H. E., Structure-Function Analyses of the N-Butanoyl L-Homoserine Lactone Quorum-Sensing Signal Define Features Critical to Activity in RhIR. *ACS Chem. Biol.* **2018**, *13* (9), 2655-2662.

15. Welsh, M. A.; Blackwell, H. E., Chemical probes of quorum sensing: from compound development to biological discovery. *FEMS Microbiol. Rev.* **2016**, *40* (5), 774-794.
16. Daniels, R.; Reynaert, S.; Hoekstra, H.; Verreth, C.; Janssens, J.; Braeken, K.; Fauvart, M.; Beullens, S.; Heusdens, C.; Lambrechts, I.; De Vos, D. E.; Vanderleyden, J.; Vermant, J.; Michiels, J., Quorum signal molecules as biosurfactants affecting swarming in *Rhizobium etli*. *Proc. Natl. Acad. Sci. U. S. A.* **2006**, *103* (40), 14965-14970.
17. Davis, B. M.; Jensen, R.; Williams, P.; O'Shea, P., The Interaction of N-Acylhomoserine Lactone Quorum Sensing Signaling Molecules with Biological Membranes: Implications for Inter-Kingdom Signaling. *PLoS One* **2010**, *5* (10), e13522.
18. Davis, B. M.; Richens, J. L.; O'Shea, P., Label-Free Critical Micelle Concentration Determination of Bacterial Quorum Sensing Molecules. *Biophys. J.* **2011**, *101* (1), 245-254.
19. Jakubczyk, D.; Barth, C.; Kubas, A.; Anastassacos, F.; Koelsch, P.; Fink, K.; Schepers, U.; Brenner-Weiss, G.; Brase, S., Deuterium-labelled N-acyl-L-homoserine lactones (AHLs)-inter-kingdom signalling molecules-synthesis, structural studies, and interactions with model lipid membranes. *Anal. Bioanal. Chem.* **2012**, *403* (2), 473-482.
20. Barth, C.; Jakubczyk, D.; Kubas, A.; Anastassacos, F.; Brenner-Weiss, G.; Fink, K.; Schepers, U.; Brase, S.; Koelsch, P., Interkingdom Signaling: Integration, Conformation, and Orientation of N-Acyl-L-homoserine Lactones in Supported Lipid Bilayers. *Langmuir* **2012**, *28* (22), 8456-8462.
21. Lentini, R.; Martin, N. Y.; Forlin, M.; Belmonte, L.; Fontana, J.; Cornella, M.; Martini, L.; Tamburini, S.; Bentley, W. E.; Jousson, O.; Mansy, S. S., Two-Way Chemical Communication between Artificial and Natural Cells. *ACS Cent. Sci.* **2017**, *3* (2), 117-123.
22. Song, D. K.; Meng, J. C.; Cheng, J.; Fan, Z.; Chen, P. Y.; Ruan, H. F.; Tu, Z. Y.; Kang, N.; Li, N.; Xu, Y.; Wang, X. B.; Shi, F.; Mu, L. B.; Li, T. F.; Ren, W. R.; Lin, X.; Zhu, J.; Fang, X. H.; Amrein, M. W.; Wu, W. H.; Yan, L. T.; Lu, J. H.; Xia, T.; Shi, Y., *Pseudomonas aeruginosa* quorum-sensing metabolite induces host immune cell death through cell surface lipid domain dissolution. *Nat. Microbiol.* **2019**, *4* (1), 97-111.
23. Gahan, C. G.; Patel, S. J.; Boursier, M. E.; Nyffeler, K. E.; Jennings, J.; Abbott, N. L.; Blackwell, H. E.; Van Lehn, R. C.; Lynn, D. M., Bacterial Quorum Sensing Signals Self-Assemble in Aqueous Media to Form Micelles and Vesicles: An Integrated Experimental and Molecular Dynamics Study. *J. Phys. Chem. B* **2020**, *124* (18), 3616-3628.
24. Jin, T.; Patel, S. J.; Van Lehn, R. C., Molecular simulations of lipid membrane partitioning and translocation by bacterial quorum sensing modulators. *PLoS One* **2021**, *16* (2), e0246187.

25. Gahan, C. G.; Patel, S. J.; Chen, L. M.; Manson, D. E.; Ehmer, Z. J.; Blackwell, H. E.; Van Lehn, R. C.; Lynn, D. M., Bacterial Quorum Sensing Signals Promote Large-Scale Remodeling of Lipid Membranes. *Langmuir* **2021**, *37*, 9120–9136.
26. Yates, E. A.; Philipp, B.; Buckley, C.; Atkinson, S.; Chhabra, S. R.; Sockett, R. E.; Goldner, M.; Dessaux, Y.; Camara, M.; Smith, H.; Williams, P., N-acylhomoserine Lactones undergo lactonolysis in a pH-, temperature-, and acyl chain length-dependent manner during growth of *Yersinia pseudotuberculosis* and *Pseudomonas aeruginosa*. *Infect. Immun.* **2002**, *70* (10), 5635-5646.
27. Wang, L. H.; Weng, L. X.; Dong, Y. H.; Zhang, L. H., Specificity and enzyme kinetics of the quorum-quenching N-acyl homoserine lactone lactonase (AHL-lactonase). *J. Biol. Chem.* **2004**, *279* (14), 13645-13651.
28. Hodgkinson, J. T.; Galloway, W.; Casoli, M.; Keane, H.; Su, X. B.; Salmond, G. P. C.; Welch, M.; Spring, D. R., Robust routes for the synthesis of N-acylated-L-homoserine lactone (AHL) quorum sensing molecules with high levels of enantiomeric purity. *Tetrahedron Lett.* **2011**, *52* (26), 3291-3294.
29. Kolahdouzan, K.; Jackman, J. A.; Yoon, B. K.; Kim, M. C.; Johal, M. S.; Cho, N. J., Optimizing the Formation of Supported Lipid Bilayers from Bicellar Mixtures. *Langmuir* **2017**, *33* (20), 5052-5064.
30. Mayer, L. D.; Hope, M. J.; Cullis, P. R., Vesicles of variable sizes produced by a rapid extrusion procedure. *Biochim. Biophys. Acta* **1986**, *858* (1), 161-168.
31. Lapinski, M. M.; Castro-Forero, A.; Greiner, A. J.; Ofoli, R. Y.; Blanchard, G. J., Comparison of liposomes formed by sonication and extrusion: Rotational and translational diffusion of an embedded chromophore. *Langmuir* **2007**, *23* (23), 11677-11683.
32. Lee, M. R.; Raman, N.; Ortiz-Bermudez, P.; Lynn, D. M.; Palecek, S. P., 14-Helical Beta-Peptides Elicit Toxicity against *C. albicans* by Forming Pores in the Cell Membrane and Subsequently Disrupting Intracellular Organelles. *Cell Chem. Biol.* **2019**, *26* (2), 289-299.
33. Lichtenberg, D.; Ahyayauch, H.; Alonso, A.; Goni, F. M., Detergent solubilization of lipid bilayers: a balance of driving forces. *Trends Biochem. Sci.* **2013**, *38* (2), 85-93.
34. Powney, J.; Addison, C. C., The properties of detergent solutions. *Trans. Faraday Soc.* **1937**, *33* (2), 1243-1259.
35. Yoon, B. K.; Jackman, J. A.; Kim, M. C.; Sut, T. N.; Cho, N. J., Correlating Membrane Morphological Responses with Micellar Aggregation Behavior of Capric Acid and Monocaprin. *Langmuir* **2017**, *33* (11), 2750-2759.

36. Kim, M. C.; Gunnarsson, A.; Tabaei, S. R.; Hook, F.; Cho, N. J., Supported lipid bilayer repair mediated by AH peptide. *Phys. Chem. Chem. Phys.* **2016**, *18* (4), 3040-3047.
37. Yoon, B. K.; Park, S.; Ma, G. J.; Kolahdouzan, K.; Zhdanov, V. P.; Jackman, J. A.; Cho, N. J., Competing Interactions of Fatty Acids and Monoglycerides Trigger Synergistic Phospholipid Membrane Remodeling. *J. Phys. Chem. Lett.* **2020**, *11* (13), 4951-4957.
38. Yoon, B. K.; Jackman, J. A.; Kim, M. C.; Cho, N. J., Spectrum of Membrane Morphological Responses to Antibacterial Fatty Acids and Related Surfactants. *Langmuir* **2015**, *31* (37), 10223-10232.
39. Yoon, B. K.; Jackman, J. A.; Park, S.; Mokrzecka, N.; Cho, N. J., Characterizing the Membrane-Disruptive Behavior of Dodecylglycerol Using Supported Lipid Bilayers. *Langmuir* **2019**, *35* (9), 3568-3575.
40. Yoon, B. K.; Park, H.; Zhdanov, V. P.; Jackman, J. A.; Cho, N.-J., Real-time nanoplasmonic sensing of three-dimensional morphological changes in a supported lipid bilayer and antimicrobial testing applications. *Biosens. Bioelectron.* **2021**, *174*, 112768.
41. Heerklotz, H., Membrane stress and permeabilization induced by asymmetric incorporation of compounds. *Biophys. J.* **2001**, *81* (1), 184-195.
42. Heerklotz, H., Interactions of surfactants with lipid membranes. *Q. Rev. Biophys.* **2008**, *41* (3-4), 205-264.
43. Lichtenberg, D.; Ahyayauch, H.; Goni, F. M., The Mechanism of Detergent Solubilization of Lipid Bilayers. *Biophys. J.* **2013**, *105* (2), 289-299.
44. Binder, H.; Lindblom, G., Charge-dependent translocation of the Trojan peptide penetratin across lipid membranes. *Biophys. J.* **2003**, *85* (2), 982-995.
45. Heerklotz, H.; Seelig, J., Leakage and lysis of lipid membranes induced by the lipopeptide surfactin. *Eur. Biophys. J.* **2007**, *36* (4-5), 305-314.
46. Zaragoza, A.; Aranda, F. J.; Espuny, M. J.; Teruel, J. A.; Marques, A.; Manresa, A.; Ortiz, A., Mechanism of Membrane Permeabilization by a Bacterial Trehalose Lipid Biosurfactant Produced by *Rhodococcus sp.* *Langmuir* **2009**, *25* (14), 7892-7898.
47. Chhabra, S. R.; Harty, C.; Hooi, D. S. W.; Daykin, M.; Williams, P.; Telford, G.; Pritchard, D. I.; Bycroft, B. W., Synthetic analogues of the bacterial signal (quorum sensing) molecule N-(3-oxododecanoyl)-L-homoserine lactone as immune modulators. *J. Med. Chem.* **2003**, *46* (1), 97-104.
48. Liu, Y. C.; Chan, K. G.; Chang, C. Y., Modulation of Host Biology by *Pseudomonas aeruginosa* Quorum Sensing Signal Molecules: Messengers or Traitors. *Front. Microbiol.* **2015**, *6*, 1226.

For Table of Contents Use Only:

